ADVANCED OPTICAL MATERIALS
www.advopticalmat.de

Liquid Crystalline Order and Electric Switching of Upconversion Luminescence in Colloidal Nanorod Suspensions

*Sungoh Park, Haridas Mundoor, Blaise Fleury, Patrick Davidson, Jao van de Lagemaat, and Ivan I. Smalyukh**

The polarization-dependent photon upconversion luminescence properties of large-scale orientationally ordered soft matter systems formed by colloidal nanorods dispersed in an isotropic solvent are studied. The electrostatically charged photon-upconverting nanorods form an isotropic dispersion at low concentrations, whereas orientational order and a nematic phase emerge at high concentrations. When an alternating electric field is applied, particles align in the direction of the electric field in both nematic and isotropic phases, though the nature of this electric switching is different in these two phases. Owing to the long-range orientational order in the nematic phase, the upconversion luminescence from the particles is polarized without an external field. Polarization dependence of these properties can also be electrically induced in an isotropic phase of the colloidal nanorods. Further, the dynamics of switching of photon upconversion luminescence in both nematic and isotropic dispersions are explored and their potential technological uses are dicussed.

1. Introduction

Photon-upconverting materials, which can convert infrared light to visible light, have been gathering increasing interest due to their unique optical properties, namely large anti-Stokes shifts, nonblinking emission, and high photochemical stability, which can be advantageous to many applications ranging from biological deep-tissue imaging[1] to high-efficiency solar cells[2] and microscale lasers.[3] Typical methods for synthesis of upconversion nanomaterials involve replacement of a few cations from solid nanocrystalline material with rare-earth ions, such as erbium (Er^{3+}), to introduce excited metastable states. They are codoped with sensitizer cations with larger absorption cross-section, such as ytterbium (Yb^{3+}), to increase the efficiency of the upconversion process. Owing to the polarized luminescence in the visible region,[4] upconversion nanoparticles have been envisaged to have potential applications in display devices. Polarized upconversion emission arises from the crystal field interactions of the host matrix with the lanthanide ions, influenced by the local crystal symmetry of the crystalline matrix surrounding the luminescent ions.[4,5] Although upconversion particles possess desirable properties for their use in optical devices, they pose a major challenge due to the low quantum efficiency of the upconversion process, which necessitates the use of high concentrations of particles for any practical applications. Furthermore, controlling the optical response of such a large number of nanoparticles is critical for their applications in optical devices. In this regard, recently, upconversion nanorods (UCNR) were aligned in an anisotropic matrix, like nematic liquid crystals or a liquid-crystalline polymer network, providing a way to polarize and modulate the upconversion luminescence emission in a composite material.[5–7]

We propose to take advantage of the anisotropic shape of the nanoparticles to reveal their anisotropic physical properties as an ensemble. When dispersed in a solvent at a higher concentration, it is well known that high-aspect-ratio nanorods can spontaneously form a lyotropic nematic liquid-crystalline phase.[8–12] In this case, orientational

S. Park, Dr. H. Mundoor, Dr. B. Fleury, Dr. J. van de Lagemaat, Prof. I. I. Smalyukh
Department of Physics
University of Colorado
Boulder, CO 80309, USA
E-mail: ivan.smalyukh@colorado.edu
Dr. P. Davidson
Laboratoire de Physique des Solides
CNRS
Université Paris-Sud
Université Paris-Saclay
91405 Orsay, France
Dr. J. van de Lagemaat
National Renewable Energy Laboratory
Golden, CO 80401, USA
Dr. J. van de Lagemaat, Prof. I. I. Smalyukh
Renewable and Sustainable Energy Institute
National Renewable Energy Laboratory and University of Colorado
Boulder, CO 80309, USA
Prof. I. I. Smalyukh
Department of Electrical
Computer and Energy Engineering
Materials Science Engineering Program, and Soft Materials
Research Center
University of Colorado
Boulder, CO 80309, USA
The ORCID identification number(s) for the author(s) of this article can be found under https://doi.org/10.1002/adom.201900041.

DOI: 10.1002/adom.201900041

order of the particles naturally arises from the interactions between nanorods in the isotropic solvent rather than from their confinement and aligning surface interactions in an anisotropic matrix. Moreover, dispersions of nanorods in a solvent usually show a strong response to the application of an alternating electric field.[13–16] In the nematic phase, the director aligns along or perpendicular to the electric field direction (depending on dielectric anisotropy), whereas, in the isotropic phase at a lower concentration, the electric field induces the orientational order of the nanorods.[11] In this article, we demonstrate the electric switching and polarization-dependent luminescence of nematically ordered suspensions of UCNR in an isotropic medium. Further, we demonstrate the electric switching of the nematic director and the emergence of orientational order in the low concentration isotropic dispersion of the nanorods induced by the external electric field. We also establish that the upconversion luminescence emission of the particles forming the nematic phase is strongly polarized. Finally, we show how the upconversion luminescence can easily be switched and modulated by applying an electric field and discuss potential applications. More generally, we demonstrate how tunable properties of mesostructured composite materials can be designed by combining properties of individual nanoparticles with the emergent soft matter behavior in the form of long-range orientational order and facile electric switching.

2. Results and Discussion

2.1. Upconversion Nanorods and Their Properties

The slender β-$NaYF_4$:Yb/Er nanorods used in this study have been designed to form a lyotropic liquid-crystalline phase when dispersed in a solvent at high concentrations. Transmission electron microscopy (TEM) images reveal their highly anisotropic shape (**Figure 1**a). In addition, the particles were treated with hydrochloric acid (HCl) to improve the colloidal stability of the suspensions by electrostatic stabilization and to further increase the aspect ratio of these particles (Figure 1a,b). Indeed, the as-synthesized particles had a length $L \approx 1.6$ µm and diameter $D \approx 40$ nm, whereas they were ≈1.6 µm long and ≈20 nm in diameter after the acid treatment (Figure 1a,b). Stable colloidal suspensions were produced by dispersing the nanorods in ethanol. Moreover, when filled into capillaries, the suspensions spontaneously showed the coexistence of an isotropic phase at the top and a nematic phase at the bottom of a vertically oriented capillary, as expected for such slender nanorods.

The UCNR's photon upconverting properties are illustrated in Figure 1c, which shows a typical Er^{3+} emission spectrum. A drop of a very dilute dispersion was deposited on a substrate and dried to probe the polarization of the emission at the single particle level with an analyzer **A**. A single nanorod was excited, and its upconversion luminescence was collected while the angle between the nanorod's long axis and **A** was varied. The

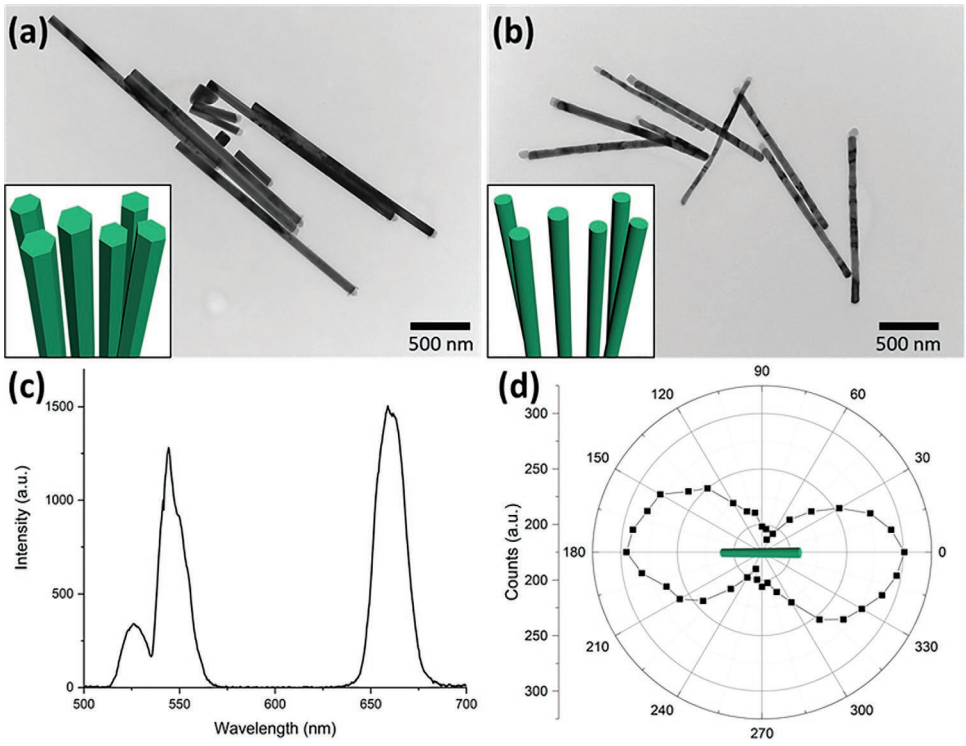

Figure 1. a,b) TEM micrograph of $NaYF_4$:Yb, Er colloidal UCNR before the acid treatment (a) and after the acid treatment (b). The insets in (a) and (b) are the schematics depicting the shapes of the rods before and after the acid treatment. c) Typical photon-upconversion luminescence spectrum of the UCNRs, where a 980 nm diode laser was used as excitation source. d) The polarization of upconversion luminescence from a single particle at 658 nm emission where the analyzer is rotated from 0° to 360°. The angle is measured between the long axis of the UCNR and the analyzer. Schematic at the center of the polar plot shows the nanorod direction.

polar plot of the emission peak at 658 nm demonstrates that the upconversion luminescence is strongly polarized (Figure 1d).

2.2. Electro-Optic Effects in the Isotropic Phase of UCNR Suspensions

We now discuss the influence of an electric field **E** on the isotropic phase of UCNR suspensions in ethanol. In the absence of a field, the nanorods are randomly oriented. Hence, the isotropic phase appears dark between crossed polarizer **P** and analyzer **A** (**Figure 2**a). However, when **E** is applied, the nanorods tend to align parallel to the field. This gives rise to a field-induced birefringence, which is detected by the transmission of light through the sample placed between crossed polarizers (Figure 2b). This field-induced birefringence strongly depends on the magnitude of **E**.

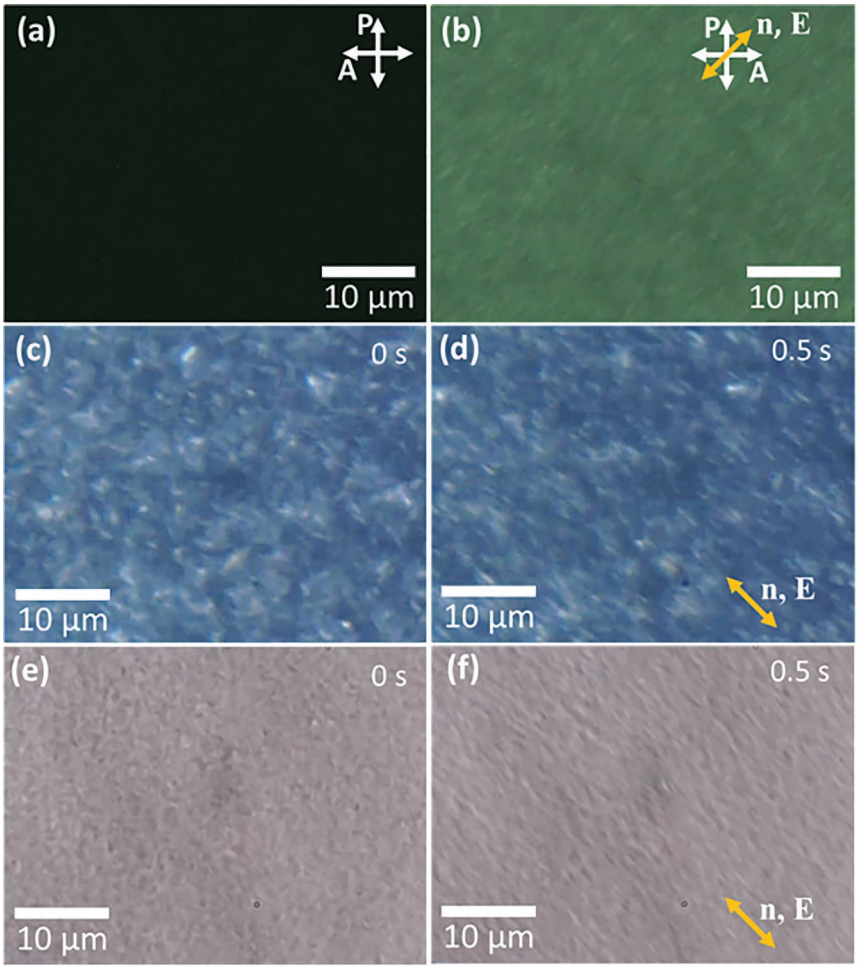

Figure 2. Polarized-light, darkfield, and brightfield optical micrographs of a colloidal UCNR suspension in isotropic phase with in-plane electric field **E** applied at 45° relative to the polarizer **P** and analyzer **A**. a) Polarized-light micrograph without **E**. There is nearly no visible-light optical transmission because of the random orientation of the nanorods. b) Polarized-light micrograph with **E**. Note that there is a significant visible-light optical transmission due to the field-induced birefringence arising from the nanorods aligned parallel to **E**. c,d) Darkfield micrographs with **E** off and on, respectively. e,f) Brightfield micrographs with **E** off and on, respectively. Images in (c,e) show random orientations of the nanorods whereas images in (d,f) reveal the alignment of the nanorods along **E**.

Darkfield and brightfield microscopies were also used to establish that the rods align parallel to **E** (Figure 2c–f). Both techniques allow for a direct imaging of the highly anisotropic nanorods, which are long enough for their orientations to be optically resolved when using high magnification microscope objectives with high (NA = 1.4) numerical aperture. The nanorod alignment direction and the degree of ordering induced by **E** can then be directly assessed using the micrographs depicted in Figure 2d,f.

In the dilute isotropic phase, we observed that the rods aligned along the field within a time scale of roughly a second. To study this phenomenon more precisely, we monitored the output of a photodiode, measuring the intensity of the light transmitted through the sample (see Experimental Section). The transmission signal showed a sharp rise and fall as **E** was switched on and off (**Figure 3**a). Fitting the rising curve to a biexponential function, $I(t) = I_0 + A\exp[-(t-t_0)/\tau_1] + B\exp[-(t-t_0)/\tau_2]$ yields two characteristic times $\tau_1 = 0.97$ s and $\tau_2 = 3.83$ s. The faster component τ_1 is consistent with a simple estimate of the rotational diffusion constant, $D_r \approx 3.3\ s^{-1}$ using the equation $\pi\eta_0 L^3 D_r/3k_B T = \ln p + \delta_\perp$ where $\delta_\perp = -0.662 + 0.917/p + 0.100/p^2$,[17] yielding ≈0.31 s for the characteristic decay time (see also Figure S1a in the Supporting Information). The slower component is probably due to hydrodynamic flows induced by sample heating that was observed causing flows and textural changes with slow relaxation.

The time evolution of the upconversion luminescence intensity at 658 nm, measured after **A** (see Experimental Section), shows the comparable sharp rise and fall in response to switching as the field was turned on and off (Figure 3b). The rising part of the curve was fitted with a single exponential function $I(t) = I_0 + A(1-\exp[-(t-t_0)/\tau])$, yielding a characteristic time $\tau = 0.9$ s, in good agreement with the fast time derived above from the evolution of the optical transmission. This good agreement confirms that the polarization dependence of the upconversion luminescence is determined by the nanorod orientation. Moreover, the use of a polarizer in the detection channel provides a way of controlling the emission intensity simply by tuning **E**.

2.3. Electro-Optic Effects in the Nematic Phase of UCNR Suspensions

Characterization of the electro-optic properties of the nematic phase of the UCNR suspensions showed different behaviors compared to that of the isotropic phase because it is spontaneously birefringent (*i.e.*, it exhibits an orientational order even

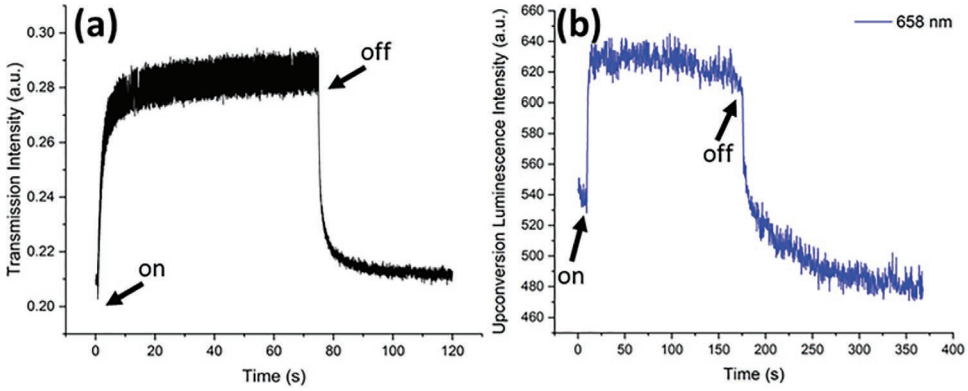

Figure 3. Time evolution of a) optical transmission intensity through the sample between crossed polarizers and b) upconversion luminescence intensity in isotropic phase colloidal UCNR suspension with the application of **E**. In (a), optical transmission intensity change is shown when a sample of colloidal UCNR suspension is placed between crossed polarizers, as the **E** at 45° with respect to crossed polarizers is switched on/off. In (b), upconversion luminescence intensity change is shown as **E** is switched on/off. The on and off timings of **E** are indicated with black arrows.

in the absence of field). The nematic phase causes no optical transmission when the sample is placed between crossed polarizers, and the nematic director (**n**) is initially parallel to **P** as shown in **Figure 4**a. However, applying **E** at 45° with respect to **P** or **A** results in the reorientation of the director **n**. This gives rise to a strong optical transmission through the sample placed between crossed polarizers (Figure 4b).

Furthermore, by adding a 530 nm full-wavelength (λ) retardation plate, the reorientation of **n** can be characterized through probing the change in the polarized interference colors. We set the initial orientation of the director $\mathbf{n}_i$ (at 45° to **P** or **A**) by applying a weak magnetic field (100–200 mT), as the nanorods tend to align perpendicular to the magnetic field (Figure 4c). As **E** was applied in the direction perpendicular to $\mathbf{n}_i$, we observed that the rods realigned along the field in about 15 s (Figure 4c–f). The time evolution of the optical transmission measured with the photodiode in this geometry is shown in **Figure 5**a. The initial uniform orientation of the director $\mathbf{n}_i$, at 45° with respect to **P** and **A** (as in Figure 4c), results in a strong optical transmission. When **E** is switched on, the signal first sharply drops as reorientation takes place, but then it recovers its initial value when the director finally realigns along **E**, which is also at 45° with **P** and **A** (final director orientation $\mathbf{n}_f$ is shown in Figure 4f). It is worth noting that the director's reorientation is accompanied by strong backflow effects.

The time-dependent variation in the upconversion luminescence was recorded after inserting **A** in front of the detector with its axis parallel to **E**. The upconversion luminescence signal rises as the director realigns along **E**, showing that the luminescence polarization closely follows the nanorod reorientation (Figure 5b). This behavior also confirms that the polarization of the luminescence is directly related to the particle geometry and the nematic ordering direction. This feature was investigated in more detail by rotating **A** with respect to **E** where **n** is parallel to **E**. Polar plots of the upconversion luminescence emission intensity versus the angle between **A** and **n** (and **E**) are given in **Figure 6** for all three luminescence peaks shown in Figure 1c. In all cases, the upconversion luminescence is strongly polarized parallel to **n**, and hence to the average nanorod axis orientation. Furthermore, the upconversion intensity variation in the nematic phase is also affected by the medium scattering due to the high-concentration ordered arrangement of the particles. This experiment also shows that the upconversion luminescence intensity can be tuned over a large range simply by applying **E** and using a polarizer.

3. Discussion and Conclusions

While recent breakthroughs in nanoscience enabled facile synthesis of nanoparticles with properties very different from bulk materials with the same material composition,[18–20] it still remains challenging to form materials from such nanoparticles while preserving these properties. For example, polarized surface plasmon resonance properties of gold nanorods explored recently,[21] and polarized luminescence properties of the upconversion nanoparticles studied here are simply lost when they are used to form isotropic colloidal dispersions or composite materials, though they can be preserved when dispersing these shape-anisotropic particles in anisotropic nematic fluids.[5,21–23] The present study demonstrates how anisotropic optical properties of photon-upconverting nanoparticles can be preserved by forming orientationally ordered states of these nanoparticles in isotropic solvents. To do so, we synthesized high-aspect-ratio upconversion β-$NaYF_4$:Yb, Er nanorods and dispersed them in ethanol. Thanks to their high aspect ratio, resulting colloidal suspensions can form not only a common isotropic phase but also a lyotropic nematic phase. In the latter, the nematic director can be switched by applying an alternating electric field. Simultaneously, the intensity of the upconversion luminescence emission from the nanorods is also tuned with the electric field, showing that these nanorods within an ensemble-like material present a polarized upconversion emission along their nematic ordering direction. In the isotropic phase, the intensity and polarization properties of the luminescence emission can be controlled by tuning the electric field strength without changing its direction. The exciting properties of polarized photon-upconversion-based luminescence reported in this study were obtained with a much simpler system than those previously reported.[5,6,23] Usually, they consisted in

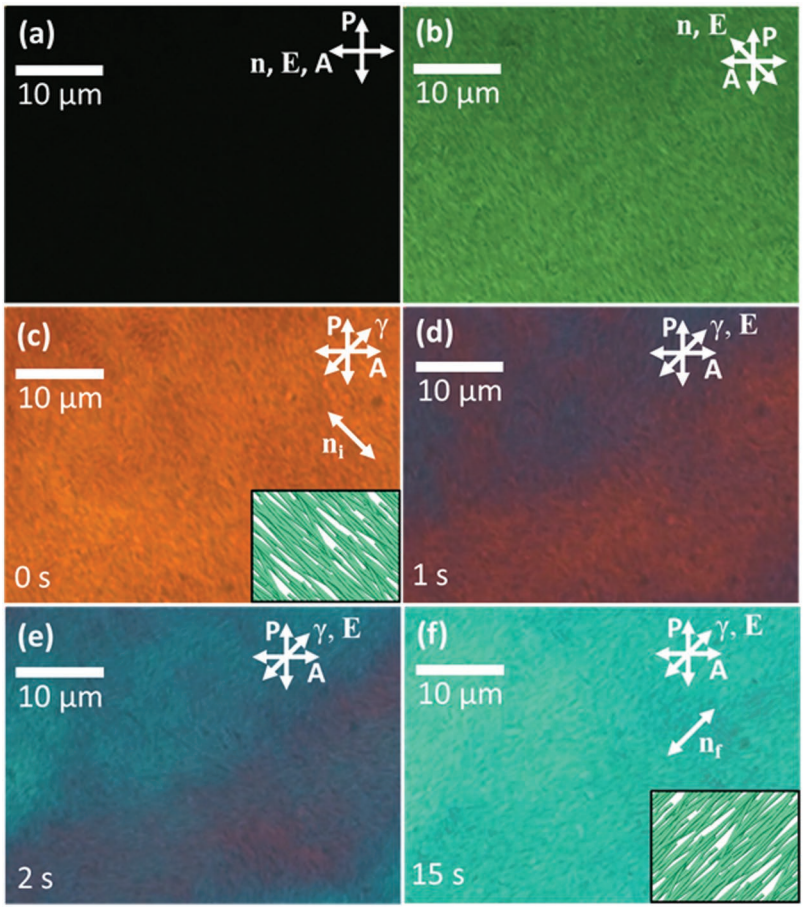

Figure 4. Polarized-light optical micrographs of a lyotropic nematic liquid-crystalline phase of a concentrated colloidal UCNR suspension when a) nematic director **n** is aligned parallel to **E** and **A** and b) **n** is aligned at 45° relative to crossed polarizers. In (a), there is no optical visible-light transmission because **n** is parallel to **A** and perpendicular to **P**. In (b), there is a strong optical transmission due to the birefringence of the liquid-crystalline phase of the colloidal dispersion. c–f) Polarized-light optical micrographs with an additional retardation plate showing the time evolution of **n** from the initial director configuration $\mathbf{n}_i$ (c) to final director configuration $\mathbf{n}_f$ (f), as **E** is applied at 45° relative to crossed polarizers. Reorientation of **n** to align parallel to **E** is demonstrated by the change of interference color from orange to blue. The initial orientation of the director $\mathbf{n}_i$ is depicted in the orientation of the rods in the schematic (inset) of (c). This is set by an external magnetic field which aligns the rods perpendicular to the field. Intermediate states where the director is undergoing reorientation are shown in (d,e). Final aligned state at the elapsed time of 15 s is shown in (f) with the director orientation $\mathbf{n}_f$, also depicted by the orientation of the rods in the schematic (inset).

nanoparticle-doped anisotropic matrices like small-molecule nematic liquid crystals or lamellar and nematic phases of surfactants and a chromonic stack of dye molecules.[5,21,22,24,25] Because of their anisotropic nature, such matrices most often require preliminary control of their macroscopic orientation by alignment layers in order to obtain monodomain samples. This technological step is no longer needed when using the UCNR suspensions in their isotropic phase. Moreover, this system, which only involves UCNRs in an isotropic solvent, does not suffer from the optical complexity related to the birefringence of an oriented matrix. Furthermore, in contrast to the doped composites, this system can have a much higher concentration of UCNRs, resulting in a stronger upconversion luminescence. While a solvent-like ethanol may be prone to evaporation, depending on the sealing of cell chambers, a large variety of other isotropic solvents can be used as host fluids for UCNR dispersions to mitigate this problem. All these features make UCNR colloidal dispersions quite promising for use in electro-optic and photonic devices.

Facile responses of our anisotropic composite materials are of interest for many applications, ranging from smart windows to displays and solar cell technologies. For example, one can envisage how switchable conversion of infrared to visible light could be used in window-based solar concentrators to enable both the electric control of solar gain and generation of electricity. In typically quantum-dot-based or fluorescent-dye-based solar concentrators,[26–30] the main idea is to convert some of the visible solar radiation passing through a window into electricity by channeling (with the help of total internal reflection and anisotropic emission) the fluorescence light into the edges of the window where efficient solar cells are located and where this light is converted into electricity.[26–29] The UCNRs would allow for the light-to-electricity conversion of solar radiation from outside of the visible range, thus not compromising visible transparency of the windows. Moreover, the infrared component of solar radiation often constitutes 50% of incoming solar energy and contributes to the high air conditioning costs in hot climates. By converting it to electricity, one can envisage not only the reduction of building energy costs due to the so-called solar gain control but also energy generation stemming from the conversion of solar energy to electricity at the edges of windows with solar concentrators. In this regard, recent reports demonstrate how the photoconversion efficiency can be enhanced by incorporating upconversion nanoparticles as spectral concentrators in solar cells.[31,32] The facile electric switching demonstrated in this work promises smart optimization of these processes depending on the desired and actual thermal environment of the building interior, season and daytime, climate conditions, etc. While the switching speed is relatively slow (with the response times in the range of ≈1 s), it is rather adequate for such smart window applications. Similarly, while absorption and luminescence have narrow spectral range characteristics, which limits efficiency and technological utility of the studied colloidal systems, colloidal codispersions of different nanoparticles with different ion doping and matrix compositions can be designed to mitigate this issue and to both tune emission spectral bands and make infrared absorption spectrally broader, although significant research is needed to optimize the chemical parameters required for designing such particles.[33–35]

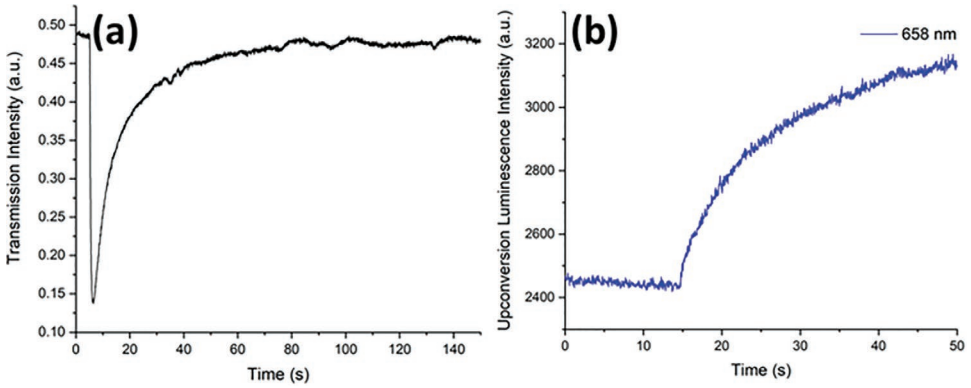

Figure 5. Time evolution of a) optical transmission intensity through the sample between crossed polarizers and b) upconversion luminescence intensity in nematic phase colloidal UCNR suspension, where in both (a,b) **n** is initially (at $t = 0$) perpendicular to **E** and then switched parallel to **E**. Optical transmission intensity (a) is measured with $\mathbf{n}_i$ at 45° with respect to crossed polarizers, and **E** is applied perpendicular to $\mathbf{n}_i$ but still at 45° to crossed polarizers. Upconversion luminescence (b) is measured through **A** parallel to **E**.

To conclude, we have developed a new breed of photon-upconverting liquid-crystalline materials with facile responses to external electric and magnetic fields. Polarization-dependent photon-upconversion-based luminescence in these materials can be tuned by low-voltage electric fields and is of interest for a large variety of applications, ranging from electro-optic and photonic devices to dynamic smart windows and solar cells.

4. Experimental Section

Materials Used: The chemicals used for synthesis, ytterbium nitrate hexahydrate [$Yb(NO_3)_3$, $6H_2O$], yttrium nitrate hexahydrate [$Y(NO_3)_3$, $6H_2O$], erbium nitrate pentahydrate [$Er(NO_3)_3$, $5H_2O$], sodium fluoride (NaF), and oleic acid were all purchased from Sigma Aldrich. Sodium hydroxide (NaOH) was purchased from Alfa Aesar. HCl, which was used for acid treatment, was purchased from Fisher Scientific.

Synthesis and Acid Treatment: The particles used in this study were β-$NaYF_4$:Yb/Er nanorods designed to exhibit efficient photon-upconversion luminescence when excited with infrared light at 980 nm. They were synthesized following a hydrothermal method reported earlier.[36] Briefly, NaOH (1.2 g) was dissolved in deionized (5 mL) water and mixed with ethanol (7 mL). Oleic acid (20 mL) was mixed with the solution. Next, NaF solution (8 mL, 1 M) was added and mixed. Then, yttrium nitrate hexahydrate (950 µL, 0.5 M), ytterbium nitrate hexahydrate (225 µL, 0.2 M), and erbium nitrate pentahydrate (50 µL, 0.2 M) solutions were added. The mixture was transferred to a 50 mL Teflon-lined autoclave, kept under vigorous stirring for 20 min, and then heated to 190 °C in an oven (OGH60, Heratherm). After 24 h, the mixture was allowed to cool down to room temperature. Subsequently, the particles deposited at the bottom of the Teflon chamber were collected and washed with deionized water and ethanol three times, and then redispersed in cyclohexane. The quantum yield of the acid-treated UCNR particles was estimated to be ≈0.1%.[33]

The UCNR nanoparticles were treated with HCl to improve the quality of the dispersion through surface charging and to further increase their aspect ratio.[6] During the acid treatment, the oleic acid ligands were removed from the particles by protonation, leaving the surfaces of the particles positively charged. In the first step, UCNR dispersions (4 mL) in cyclohexane and HCl (2 mL, 3.8 wt%) aqueous solutions were typically transferred to 20 mL glass vials and kept under stirring overnight. The particles that were initially dispersed in cyclohexane were transferred to the aqueous phase, leaving the free oleic acid molecules in cyclohexane. After the reaction, the particles were collected and washed with water and ethanol. To ensure the complete removal of the oleic acid from the particles, this acid treatment was repeated 3 times, where the second and third acid treatment durations were 12 and 3–4 h, respectively. Owing to the electrostatic stabilization, the acid-treated particles were easily dispersed in solvents such as ethanol and water, with no signs of any aggregation. The acid treatment also eroded the particles, making them more slender and slightly shorter, effectively increasing the aspect ratio of the UCNRs, which was key to achieving nematic ordering in the used isotropic fluid hosts.

TEM was used to characterize the shapes and dimensions of the UCNRs. For TEM studies, a dilute UCNR suspension in ethanol was

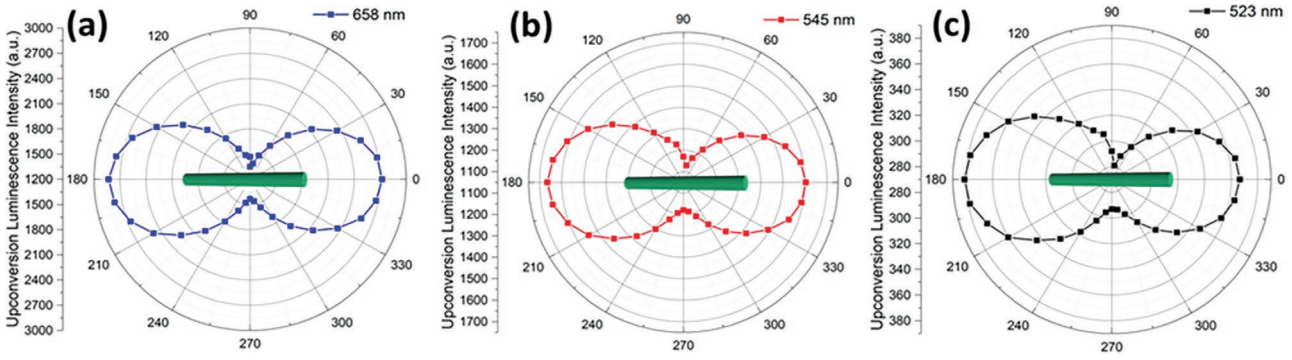

Figure 6. a) Polar plots of upconversion luminescence intensity from the nematic phase of a UCNR dispersion, corresponding to the 0°–360° rotation of the analyzer relative to the director showing the intensity variations for luminescence peak at a) 658, b) 545, and c) 523 nm. The angle is measured between the nematic director and the analyzer. Schematics at the center of the polar plots show the alignment direction of the rods.

typically deposited on a formvar-coated TEM grid and dried. TEM images were then collected using an FEI Tecnai T12 microscope operating at 120 kV.

Sample Preparation and Optical Characterization: UCNR dispersions in ethanol were filled into 0.05 × 1.00 mm or 0.10 × 2.00 mm flat glass capillaries (purchased from VitroCom, NJ) that were sealed promptly with fast-set epoxy. The capillaries were stored upright in order to create a concentration gradient due to gravity, taking advantage of the relatively small gravitational length: $l_g = k_B T/(gV\Delta\rho) = 231$ µm (where k_B is the Boltzmann constant, T is the temperature, g is the gravitational acceleration, V is the particle volume, and $\Delta\rho$ is the specific mass density contrast of the particle with the solvent). The volume fraction in the nematic phase was estimated to be in the range 11–29%, depending on the capillary region.

For electro-optic experiments, thin aluminum foil strips (≈30 µm thick), wrapped around the capillary tube, were used as electrodes while leaving a 1–2 mm gap in-between. The external electric field **E** was applied between the electrodes by a function generator (GFG-8216A, GW Instek) and an amplifier (Model 7600, Krohn-Hite). A sinusoidal voltage (V_{rms} = 100 V, f = 1 MHz) was applied between the electrodes. Response time measurements were made by monitoring the optical transmission of the sample placed between crossed polarizers, using a Si-based photodiode (PDA100A, Thorlabs) located after **A**, or, alternatively, by probing the photon upconversion luminescence under similar conditions. **E** was typically applied at an angle of 45° with respect to the directions of **P** and **A**. The voltage output from the photodiode was recorded, at a rate of 100 Hz, with a homemade software written in Labview.

Polarized-light, brightfield, and darkfield microscopy images were obtained using an inverted optical microscope (Olympus IX-81) and a charge-coupled device (CCD) camera (Flea-col, Pointgrey). Polarized-light and brightfield micrographs were acquired with a 100× objective lens with a numerical aperture NA = 1.4 (UPlanSApo, Olympus), whereas the darkfield micrographs were acquired with a 100× objective lens with variable numerical aperture NA = 0.6–1.3 (UPlanFL N, Olympus) and also using a specialized darkfield condenser with NA = 1.2–1.4 (U-DCW, Olympus).

For upconversion luminescence characterizations, an unpolarized infrared (980 nm) continuous-wave laser (purchased from Laserlands) was used as the excitation source. The excitation laser beam was focused onto the sample by a 100× objective lens (NA = 1.4), and the upconversion luminescence was collected using the same objective lens in epi-detection geometry. The estimated power density of the excitation laser at the sample plane was 54 Wcm^{-2}. The luminescence signal was sent through a 720 nm low-pass filter (FF01-720/SP, Semrock) to ensure that the signal collected was only due to the particle luminescence, and then sent to a spectrometer (USB2000, Ocean Optics). Moreover, to probe the polarization dependence of the photon-upconversion luminescence, **A** was placed after the sample with its axis parallel to **E**.

Supporting Information

Supporting Information is available from the Wiley Online Library or from the author.

Acknowledgements

The authors acknowledge the support of the Division of Chemical Sciences, Geosciences, and Biosciences, Office of Basic Energy Sciences of the U.S. Department of Energy under Contract No. DE-AC36-08GO28308 with the National Renewable Energy Laboratory (S.P., H.M., J. vdL., and I.I.S.). The views expressed in this Manuscript do not necessarily represent the views of the DOE or the U.S. Government. The authors thank Claire Goldmann, Qingkun Liu, Mahmoud Alamansouri, Enid Cruz, Bohdan Senyuk, and Yong Xie for helpful discussions and technical assistance. I.I.S. thanks CNRS for enabling a visit and an extended stay at LPS, University of Paris-Sud, France.

Conflict of Interest

The authors declare no conflict of interest.

Keywords

electric switching, lyotropic liquid crystals, polarized emission, upconversion nanoparticles

Received: January 8, 2019
Revised: January 30, 2019
Published online: February 18, 2019

[1] Z. H. Li, H. X. Miao, Y. Fu, Y. X. Liu, R. Zhang, B. Tang, *Nanoscale Res. Lett.* **2016**, *11*, 441.
[2] A. Shalav, B. S. Richards, T. Trupke, K. W. Kramer, H. U. Gudel, *Appl. Phys. Lett.* **2005**, *86*, 013505.
[3] A. Fernandez-Bravo, K. Yao, E. S. Barnard, N. J. Borys, E. S. Levy, B. Tian, C. A. Tajon, L. Moretti, M. V. Altoe, S. Aloni, K. Beketayev, F. Scotognella, B. E. Cohen, E. M. Chan, P. J. Schuck, *Nat. Nanotechnol.* **2018**, *13*, 572.
[4] J. Zhou, G. Chen, E. Wu, G. Bi, B. Wu, Y. Teng, S. Zhou, J. Qiu, *Nano Lett.* **2013**, *13*, 2241.
[5] H. Mundoor, I. I. Smalyukh, *Small* **2015**, *11*, 5572.
[6] H. Mundoor, S. Park, B. Senyuk, H. H. Wensink, I. I. Smalyukh, *Science* **2018**, *360*, 768.
[7] S. M. Ye, Y. X. Teng, A. Juan, J. Wei, L. Y. Wang, J. B. Guo, *Adv. Opt. Mater.* **2017**, *5*, 1600956.
[8] L. Onsager, *Ann. N. Y. Acad. Sci.* **1949**, *51*, 627.
[9] G. J. Vroege, H. N. W. Lekkerkerker, *Rep. Prog. Phys.* **1992**, *55*, 1241.
[10] Z. Dogic, S. Fraden, *Curr. Opin. Colloid Interface Sci.* **2006**, *11*, 47.
[11] P. Davidson, J. C. P. Gabriel, *Curr. Opin. Colloid Interface Sci.* **2005**, *9*, 377.
[12] E. Grelet, *Phys. Rev. X* **2014**, *4*, 021053.
[13] B. J. Lemaire, P. Davidson, D. Petermann, P. Panine, I. Dozov, D. Stoenescu, J. P. Jolivet, *Eur. Phys. J. E* **2004**, *13*, 309.
[14] A. de la Cotte, P. Merzeau, J. W. Kim, K. Lahlil, J. P. Boilot, T. Gacoin, E. Grelet, *Soft Matter* **2015**, *11*, 6595.
[15] J. Kim, A. de la Cotte, R. Deloncle, S. Archambeau, C. Biver, J. P. Cano, K. Lahlil, J. P. Boilot, E. Grelet, T. Gacoin, *Adv. Funct. Mater.* **2012**, *22*, 4949.
[16] E. Paineau, M. E. M. Krapf, M. S. Amara, N. V. Matskova, I. Dozov, S. Rouziere, A. Thill, P. Launois, P. Davidson, *Nat. Commun.* **2016**, *7*, 10271.
[17] M. M. Tirado, C. L. Martinez, J. G. Delatorre, *J. Chem. Phys.* **1984**, *81*, 2047.
[18] P. X. Zhao, N. Li, D. Astruc, *Coord. Chem. Rev.* **2013**, *257*, 638.
[19] V. Amendola, R. Pilot, M. Frasconi, O. M. Marago, M. A. Iati, *J. Phys.: Condens. Matter* **2017**, *29*, 203002.
[20] D. Jariwala, V. K. Sangwan, L. J. Lauhon, T. J. Marks, M. C. Hersam, *Chem. Soc. Rev.* **2013**, *42*, 2824.
[21] Q. Liu, Y. Yuan, I. I. Smalyukh, *Nano Lett.* **2014**, *14*, 4071.
[22] Q. Liu, Y. Cui, D. Gardner, X. Li, S. He, I. I. Smalyukh, *Nano Lett.* **2010**, *10*, 1347.
[23] H. Mundoor, B. Senyuk, I. I. Smalyukh, *Science* **2016**, *352*, 69.

[24] A. S. Poulos, D. Constantin, P. Davidson, M. Imperor, B. Pansu, P. Panine, L. Nicole, C. Sanchez, *Langmuir* **2008**, *24*, 6285.
[25] N. Ould-Moussa, C. Blanc, C. Zamora-Ledezma, O. Lavrentovich, I. Smalyukh, M. Islam, A. Yodh, M. Maugey, P. Poulin, E. Anglaret, M. Nobili, *Liq. Cryst.* **2013**, *40*, 1628.
[26] M. G. Debije, P. P. C. Verbunt, *Adv. Energy Mater.* **2012**, *2*, 12.
[27] W. van Sark, K. W. J. Barnham, L. H. Slooff, A. J. Chatten, A. Buchtemann, A. Meyer, S. J. McCormack, R. Koole, D. J. Farrell, R. Bose, E. E. Bende, A. R. Burgers, T. Budel, J. Quilitz, M. Kennedy, T. Meyer, C. D. M. Donega, A. Meijerink, D. Vanmaekelbergh, *Opt. Express* **2008**, *16*, 21773.
[28] D. LaCount, D. Weingarten, N. Hu, S. E. Shaheen, J. van de Lagemaat, G. Rumbles, D. M. Walba, M. T. Lusk, *J. Phys. Chem. A* **2015**, *119*, 4009.
[29] D. H. Weingarten, M. D. LaCount, J. van de Lagemaat, G. Rumbles, M. T. Lusk, S. E. Shaheen, *Nat. Commun.* **2017**, *8*, 14808.
[30] K. Barnham, J. L. Marques, J. Hassard, P. O'Brien, *Appl. Phys. Lett.* **2000**, *76*, 1197.
[31] J. C. Goldschmidt, S. Fischer, *Adv. Opt. Mater.* **2015**, *3*, 510.
[32] S. Fischer, A. Ivaturi, P. Jakob, K. W. Krämer, R. M. Rodriguez, A. Meijerink, B. Richards, J. C. Goldschmidt, *Opt. Mater.* **2018**, *84*, 389.
[33] W. Zheng, P. Huang, D. Tu, E. Ma, H. Zhu, X. Chen, *Chem. Soc. Rev.* **2015**, *44*, 1379.
[34] C. Coluccini, A. K. Sharma, D. Merli, D. V. Griend, B. Mannucci, D. Pasini, *Dalton Trans.* **2011**, *40*, 11719.
[35] M. Caricato, C. Coluccini, D. A. V. Griend, A. Fornic, D. Pasini, *New J. Chem.* **2013**, *37*, 2792.
[36] L. Y. Wang, Y. D. Li, *Chem. Mater.* **2007**, *19*, 727.